ELSEVIER

26 September 1996

PHYSICS LETTERS B

Physics Letters B 385 (1996) 433–444

Search for unstable neutral and charged heavy leptons in e^+e^- collisions at $\sqrt{s} = 130$ and 136 GeV

OPAL Collaboration

G. Alexander[w], J. Allison[p], N. Altekamp[e], K. Ametewee[y], K.J. Anderson[i], S. Anderson[ℓ], S. Arcelli[b], S. Asai[x], D. Axen[ac], G. Azuelos[r,1], A.H. Ball[q], E. Barberio[h], R.J. Barlow[p], R. Bartoldus[c], J.R. Batley[e], J. Bechtluft[n], C. Beeston[p], T. Behnke[h], A.N. Bell[a], K.W. Bell[t], G. Bella[w], S. Bentvelsen[h], P. Berlich[j], S. Bethke[n], O. Biebel[n], V. Blobel[h], I.J. Bloodworth[a], J.E. Bloomer[a], M. Bobinski[j], P. Bock[k], H.M. Bosch[k], M. Boutemeur[ah], B.T. Bouwens[ℓ], S. Braibant[ℓ], R.M. Brown[t], H.J. Burckhart[h], C. Burgard[h], R. Bürgin[j], P. Capiluppi[b], R.K. Carnegie[f], A.A. Carter[m], J.R. Carter[e], C.Y. Chang[q], C. Charlesworth[f], D.G. Charlton[a,2], D. Chrisman[d], S.L. Chu[d], P.E.L. Clarke[o], I. Cohen[w], J.E. Conboy[o], O.C. Cooke[p], M. Cuffiani[b], S. Dado[v], C. Dallapiccola[q], G.M. Dallavalle[b], S. De Jong[ℓ], L.A. del Pozo[h], K. Desch[c], M.S. Dixit[g], E. do Couto e Silva[ℓ], M. Doucet[r], E. Duchovni[z], G. Duckeck[ah], I.P. Duerdoth[p], J.E.G. Edwards[p], P.G. Estabrooks[f], H.G. Evans[i], M. Evans[m], F. Fabbri[b], P. Fath[k], F. Fiedler[ℓ], M. Fierro[b], H.M. Fischer[c], R. Folman[z], D.G. Fong[q], M. Foucher[q], A. Fürtjes[h], P. Gagnon[g], A. Gaidot[u], J.W. Gary[d], J. Gascon[r], S.M. Gascon-Shotkin[q], N.I. Geddes[t], C. Geich-Gimbel[c], F.X. Gentit[u], T. Geralis[t], G. Giacomelli[b], P. Giacomelli[d], R. Giacomelli[b], V. Gibson[e], W.R. Gibson[m], D.M. Gingrich[ad,1], D. Glenzinski[i], J. Goldberg[v], M.J. Goodrick[e], W. Gorn[d], C. Grandi[b], E. Gross[z], M. Gruwé[h], C. Hajdu[af], G.G. Hanson[ℓ], M. Hansroul[h], M. Hapke[m], C.K. Hargrove[g], P.A. Hart[i], C. Hartmann[c], M. Hauschild[h], C.M. Hawkes[e], R. Hawkings[h], R.J. Hemingway[f], G. Herten[j], R.D. Heuer[h], M.D. Hildreth[h], J.C. Hill[e], S.J. Hillier[a], T. Hilse[j], P.R. Hobson[y], R.J. Homer[a], A.K. Honma[ab,1], D. Horváth[af,3], R. Howard[ac], R.E. Hughes-Jones[p], D.E. Hutchcroft[e], P. Igo-Kemenes[k], D.C. Imrie[y], M.R. Ingram[p], K. Ishii[x], A. Jawahery[q], P.W. Jeffreys[t], H. Jeremie[r], M. Jimack[a], A. Joly[r], C.R. Jones[e], G. Jones[p], M. Jones[f], R.W.L. Jones[h], U. Jost[k], P. Jovanovic[a], T.R. Junk[h], D. Karlen[f], K. Kawagoe[x], T. Kawamoto[x], R.K. Keeler[ab], R.G. Kellogg[q], B.W. Kennedy[t], B.J. King[h], J. Kirk[ac], S. Kluth[h], T. Kobayashi[x], M. Kobel[j], D.S. Koetke[f], T.P. Kokott[c], S. Komamiya[x], R. Kowalewski[h], T. Kress[k], P. Krieger[f], J. von Krogh[k], P. Kyberd[m], G.D. Lafferty[p], H. Lafoux[u], R. Lahmann[q], W.P. Lai[s], D. Lanske[n], J. Lauber[o], S.R. Lautenschlager[ae], J.G. Layter[d], D. Lazic[v], A.M. Lee[ae], E. Lefebvre[r], D. Lellouch[z],

PII S0370-2693(96)00963-X

J. Letts [b], L. Levinson [z], C. Lewis [o], S.L. Lloyd [m], F.K. Loebinger [p], G.D. Long [q], M.J. Losty [g], J. Ludwig [j], A. Luig [j], A. Malik [u], M. Mannelli [h], S. Marcellini [b], C. Markus [c], A.J. Martin [m], J.P. Martin [r], G. Martinez [q], T. Mashimo [x], W. Matthews [y], P. Mättig [c], W.J. McDonald [ad], J. McKenna [ac], E.A. Mckigney [o], T.J. McMahon [a], A.I. McNab [m], R.A. McPherson [h], F. Meijers [h], S. Menke [c], F.S. Merritt [i], H. Mes [g], J. Meyer [aa], A. Michelini [b], G. Mikenberg [z], D.J. Miller [o], R. Mir [z], W. Mohr [j], A. Montanari [b], T. Mori [x], M. Morii [x], U. Müller [c], K. Nagai [z], I. Nakamura [x], H.A. Neal [h], B. Nellen [c], B. Nijjhar [p], R. Nisius [h], S.W. O'Neale [a], F.G. Oakham [g], F. Odorici [b], H.O. Ogren [ℓ], T. Omori [x], M.J. Oreglia [i], S. Orito [x], J. Pálinkás [ag,4], G. Pásztor [af], J.R. Pater [p], G.N. Patrick [t], J. Patt [j], M.J. Pearce [a], S. Petzold [aa], P. Pfeifenschneider [n], J.E. Pilcher [i], J. Pinfold [ad], D.E. Plane [h], P. Poffenberger [ab], B. Poli [b], A. Posthaus [c], H. Przysiezniak [ad], D.L. Rees [a], D. Rigby [a], S.A. Robins [m], N. Rodning [ad], J.M. Roney [ab], A. Rooke [o], E. Ros [h], A.M. Rossi [b], M. Rosvick [ab], P. Routenburg [ad], Y. Rozen [v], K. Runge [j], O. Runolfsson [h], U. Ruppel [n], D.R. Rust [ℓ], R. Rylko [y], K. Sachs [j], E.K.G. Sarkisyan [w], M. Sasaki [x], C. Sbarra [b], A.D. Schaile [ah], O. Schaile [ah], F. Scharf [c], P. Scharff-Hansen [h], P. Schenk [d], B. Schmitt [h], S. Schmitt [k], M. Schröder [h], H.C. Schultz-Coulon [j], M. Schulz [h], M. Schumacher [c], P. Schütz [c], W.G. Scott [t], T.G. Shears [p], B.C. Shen [d], C.H. Shepherd-Themistocleous [aa], P. Sherwood [o], G.P. Siroli [b], A. Sittler [aa], A. Skillman [o], A. Skuja [q], A.M. Smith [h], T.J. Smith [ab], G.A. Snow [q], R. Sobie [ab], S. Söldner-Rembold [j], R.W. Springer [ad], M. Sproston [t], A. Stahl [c], M. Starks [ℓ], M. Steiert [k], K. Stephens [p], J. Steuerer [aa], B. Stockhausen [c], D. Strom [s], F. Strumia [h], P. Szymanski [t], R. Tafirout [r], S.D. Talbot [a], S. Tanaka [x], P. Taras [r], S. Tarem [v], M. Tecchio [h], M. Thiergen [j], M.A. Thomson [h], E. von Törne [c], S. Towers [f], T. Tsukamoto [x], E. Tsur [w], A.S. Turcot [i], M.F. Turner-Watson [h], P. Utzat [k], R. Van Kooten [ℓ], G. Vasseur [u], M. Verzocchi [j], P. Vikas [r], M. Vincter [ab], E.H. Vokurka [p], F. Wäckerle [j], A. Wagner [aa], C.P. Ward [e], D.R. Ward [e], J.J. Ward [o], P.M. Watkins [a], A.T. Watson [a], N.K. Watson [g], P. Weber [f], P.S. Wells [h], N. Wermes [c], J.S. White [ab], B. Wilkens [j], G.W. Wilson [aa], J.A. Wilson [a], G. Wolf [z], S. Wotton [e], T.R. Wyatt [p], S. Yamashita [x], G. Yekutieli [z], V. Zacek [r]

[a] *School of Physics and Space Research, University of Birmingham, Birmingham B15 2TT, UK*
[b] *Dipartimento di Fisica dell' Università di Bologna and INFN, I-40126 Bologna, Italy*
[c] *Physikalisches Institut, Universität Bonn, D-53115 Bonn, Germany*
[d] *Department of Physics, University of California, Riverside CA 92521, USA*
[e] *Cavendish Laboratory, Cambridge CB3 0HE, UK*
[f] *Ottawa-Carleton Institute for Physics, Department of Physics, Carleton University, Ottawa, Ontario K1S 5B6, Canada*
[g] *Centre for Research in Particle Physics, Carleton University, Ottawa, Ontario K1S 5B6, Canada*
[h] *CERN, European Organisation for Particle Physics, CH-1211 Geneva 23, Switzerland*
[i] *Enrico Fermi Institute and Department of Physics, University of Chicago, Chicago IL 60637, USA*
[j] *Fakultät für Physik, Albert Ludwigs Universität, D-79104 Freiburg, Germany*
[k] *Physikalisches Institut, Universität Heidelberg, D-69120 Heidelberg, Germany*
[ℓ] *Indiana University, Department of Physics, Swain Hall West 117, Bloomington IN 47405, USA*
[m] *Queen Mary and Westfield College, University of London, London E1 4NS, UK*
[n] *Technische Hochschule Aachen, III Physikalisches Institut, Sommerfeldstrasse 26-28, D-52056 Aachen, Germany*
[o] *University College London, London WC1E 6BT, UK*
[p] *Department of Physics, Schuster Laboratory, The University, Manchester M13 9PL, UK*
[q] *Department of Physics, University of Maryland, College Park, MD 20742, USA*

[r] Laboratoire de Physique Nucléaire, Université de Montréal, Montréal, Quebec H3C 3J7, Canada
[s] University of Oregon, Department of Physics, Eugene OR 97403, USA
[t] Rutherford Appleton Laboratory, Chilton, Didcot, Oxfordshire OX11 0QX, UK
[u] CEA, DAPNIA/SPP, CE-Saclay, F-91191 Gif-sur-Yvette, France
[v] Department of Physics, Technion-Israel Institute of Technology, Haifa 32000, Israel
[w] Department of Physics and Astronomy, Tel Aviv University, Tel Aviv 69978, Israel
[x] International Centre for Elementary Particle Physics and Department of Physics, University of Tokyo, Tokyo 113, Japan and Kobe University, Kobe 657, Japan
[y] Brunel University, Uxbridge, Middlesex UB8 3PH, UK
[z] Particle Physics Department, Weizmann Institute of Science, Rehovot 76100, Israel
[aa] Universität Hamburg/DESY, II Institut für Experimental Physik, Notkestrasse 85, D-22607 Hamburg, Germany
[ab] University of Victoria, Department of Physics, P O Box 3055, Victoria BC V8W 3P6, Canada
[ac] University of British Columbia, Department of Physics, Vancouver BC V6T 1Z1, Canada
[ad] University of Alberta, Department of Physics, Edmonton AB T6G 2J1, Canada
[ae] Duke University, Department of Physics, Durham, NC 27708-0305, USA
[af] Research Institute for Particle and Nuclear Physics, H-1525 Budapest, PO Box 49, Hungary
[ag] Institute of Nuclear Research, H-4001 Debrecen, PO Box 51, Hungary
[ah] Ludwigs-Maximilians-Universität München, Sektion Physik, Am Coulombwall 1, D-85748 Garching, Germany

Received 5 July 1996
Editor: K. Winter

Abstract

Searches for unstable neutral and charged heavy leptons (L^0, $L^\pm$) have been performed using a data sample of 2.6 pb^{-1} at a centre-of-mass energy of $\sqrt{s}$ = 130 GeV and 2.6 pb^{-1} at 136 GeV collected with the OPAL detector at LEP during November 1995. No candidate event was observed. If an unstable Dirac neutral heavy lepton L^0 decays only into eW*, μW* or τW*, the lower limits on its mass at 95% C.L. are 62.5 GeV, 63.0 GeV and 57.4 GeV, respectively. The limits are modified for a Majorana L^0 to 51.4 GeV, 52.2 GeV and 44.2 GeV, respectively. For charged heavy leptons, a lower mass limit of 64.5 GeV at 95% C.L. was obtained, if $L^\pm$ decays into a stable heavy neutrino ν_L and $W^{*\pm}$, and if $m_{L^\pm} - m_{\nu_L} > 10$ GeV. If $L^\pm$ decays through lepton flavour mixing into a massless neutrino ν_ℓ and $W^{*\pm}$, the lower limit on $m_{L^\pm}$ was determined to be 63.9 GeV at 95% C.L.

1. Introduction

This paper presents searches for pair production of unstable neutral heavy leptons $L^0\bar{L}^0$ and unstable charged heavy leptons L^+L^- in e^+e^- collisions[5]. The data used in this analysis correspond to an integrated luminosity of 2.6 pb^{-1} at a centre-of-mass energy of $\sqrt{s}$ = 130 GeV and 2.6 pb^{-1} at 136 GeV collected with the OPAL detector at LEP during November 1995.

The precise measurements of the Z boson parameters by the LEP and SLC experiments have determined the number of species of light neutrinos to be three [1]. However, this does not exclude a fourth generation in which all the fermions are heavy. The lower mass limit based on LEP running around the Z^0 peak (LEP1) for the fourth generation stable neutrino (ν_L) was 45.0 GeV for a Dirac neutrino and 39.5 GeV for a Majorana neutrino [1]. The cross-sections for the $e^+e^- \to L^0\bar{L}^0$ and $e^+e^- \to L^+L^-$ processes are given in Ref. [2].

Neutral heavy lepton pairs $L^0\bar{L}^0$ could be produced in e^+e^- annihilation via a virtual Z boson. The following decay mode was considered:
(A) $L^0 \to \ell W^*$ via lepton flavour mixing, where ℓ

[1] And at TRIUMF, Vancouver, Canada V6T 2A3
[2] And Royal Society University Research Fellow
[3] And Institute of Nuclear Research, Debrecen, Hungary
[4] And Department of Experimental Physics, Lajos Kossuth University, Debrecen, Hungary
[5] Throughout this paper, charge conjugation is implicitly assumed. L^- denotes an unstable charged heavy lepton, L^0 denotes an unstable neutral heavy lepton and ν_L denotes a stable heavy neutrino.

is e, μ or τ, and W* is a virtual W boson. The Majorana L^0 can decay into either $\ell^- W^{*+}$ or $\ell^+ W^{*-}$. Therefore the charge correlation between the two light leptons was not used in the analysis, in order to be sensitive to both Dirac and Majorana L^0. The LEP1 lower mass limit for an unstable L^0 was 45.7 GeV for a Dirac L^0 and 45.1 GeV for a Majorana L^0, if the coupling $L^0 L^0 Z^*$ is the same as for $\nu_\ell \nu_\ell Z^*$ [1,3]. The visible energy of these events is expected to be large and there should be at least four charged particles, including at least two light leptons (e, μ or τ), in an event.

Charged heavy lepton pairs L^+L^- could be produced in e^+e^- annihilation via a virtual Z^0 boson or a virtual photon. The ordinary V-A coupling was assumed for the $L^- \nu_L W^{*-}$ and $L^- \nu_\ell W^{*-}$ vertices. The following two cases were studied:

(B) $L^- \rightarrow \nu_L W^{*-}$, where ν_L is a stable heavy neutrino and assumed to be heavier than the lower mass limit from the LEP1 experiments [1,3].

(C) $L^- \rightarrow \nu_\ell W^{*-}$, where ν_ℓ is ν_e, ν_μ or ν_τ. The decay occurs via lepton flavour mixing. The experimental limit from LEP1 data was $m_{L^-} > 42.7$ GeV [1,3].

The expected experimental signature for L^+L^- events for both cases is that of a multijet[6] event with a large, unbalanced transverse momentum with respect to the beam axis. If all the visible decay products of L^- and L^+ happened to be in the same hemisphere, the event topology could be a monojet. The events in case (B) are expected to have a smaller visible energy than for case (C), because the two heavy neutrinos carry away more energy and momentum.

In this paper, L^0 and L^- were assumed to be unstable. Cascade decays ($L^0 \rightarrow L^- \rightarrow \nu_\ell$, $L^- \rightarrow L^0 \rightarrow \ell$) of heavy leptons were not considered in this analysis. The analysis was designed to have a good sensitivity for heavy leptons with a decay length shorter than about 10 cm. Namely, the mixing parameters of L^0–ν_ℓ and L^-–ℓ^- were assumed to satisfy the condition $\sum_\ell |V_{L^0\ell}|^2 > \mathcal{O}(10^{-11})$ for case (A), and $\sum_\ell |V_{L^-\nu_\ell}|^2 > \mathcal{O}(10^{-11})$ for case (C), where $V_{L^0\ell}$ is the flavour mixing parameter between a neutral heavy lepton and a light lepton (e, μ or τ) and $V_{L^-\nu_\ell}$ is the flavour mixing parameter between a charged heavy lepton and a light neutrino (ν_e, ν_μ or ν_τ).

[6] An isolated lepton is treated as a jet.

The two W* bosons in an $L^0\bar{L}^0$ or L^+L^- event can decay either leptonically or hadronically. The analysis presented here is sensitive to all the possible combinations of the decay topologies and was designed to search for heavy leptons with masses above the LEP1 experimental limits.

Other recent searches for heavy leptons are presented in [4].

2. The OPAL detector and event simulation

2.1. The OPAL detector

The OPAL detector, which is described in detail in [5], is a multipurpose apparatus having nearly complete solid angle coverage. The central detector consists of a system of tracking chambers providing charged particle tracking over 96% of the full solid angle[7] inside a uniform 0.435 T magnetic field. The solenoid is surrounded by a time-of-flight (TOF) scintillating counter array. A lead-glass electromagnetic (EM) calorimeter located outside the magnet coil covers the full azimuthal range with excellent hermeticity in the polar angle range of $|\cos\theta| < 0.82$ for the barrel region and $0.81 < |\cos\theta| < 0.984$ for the endcap region. The magnet return yoke is instrumented for hadron calorimetry (HCAL), consisting of barrel and endcap sections along with pole tips detectors that together cover the region $|\cos\theta| < 0.99$. Calorimeters close to the beam axis measure the luminosity using small angle Bhabha scattering events and complete the geometrical acceptance down to 26 mrad from the beam axis. These include the forward detectors which are lead-scintillator sandwich calorimeters and, at smaller angles, silicon tungsten calorimeters [6] located on both sides of the interaction point. The gap between the endcap EM calorimeter and the forward detector is filled by an additional lead-scintillator electromagnetic calorimeter, called the gamma-catcher.

[7] A right-handed coordinate system is adopted, where the x-axis points to the centre of the LEP ring, and positive z is along the electron beam direction. The angles θ and ϕ are the polar and azimuthal angles, respectively.

2.2. Monte Carlo event simulation

$L^0\bar{L}^0$ and L^+L^- events have been generated using the TIPTOP [7] generator, which includes the effects of spin correlations in the weak decays. The generator was modified so that JETSET 7.4 [8] could be used for the hadronization, which includes gluon radiation. Initial state photon radiation was implemented in the generator based on the calculations of Berends and Kleiss [9]. $L^0\bar{L}^0$ events were generated at six m_{L^0} values from 40 to 63 GeV for the three different final states $eW^* + eW^*$, $\mu W^* + \mu W^*$ and $\tau W^* + \tau W^*$. L^+L^- events were generated at 26 points in the (m_{L^-}, m_{ν_L}) plane for case (B) and at six m_{L^-} values from 45 to 65 GeV for case (C).

The following background processes were simulated in this analysis:

- Hadronic events with an isolated lepton coming from a heavy flavour decay, or with an isolated track misidentified as a lepton, are an important background for the L^0 search. In the L^- search, the dominant $q\bar{q}(\gamma)$ background events are multijet events with one or more poorly reconstructed jet momenta. The JETSET 7.4 [8] and PYTHIA 5.7 [8] Monte Carlo generators were used for multihadron events.
- The KORALZ [10] event generator was used for the generation of $\tau^+\tau^-(\gamma)$ and $\mu^+\mu^-(\gamma)$ events. A sample of $e^+e^-(\gamma)$ events was generated using the BABAMC generator [11]. Radiative and non-radiative τ pairs are a potential source of background for the topology of two acoplanar jets, because neutrinos from the τ decays carry away energy and momentum.
- In case (B), particularly for a small mass difference between L^- and ν_L, events from two-photon processes are the main background. Since the visible energy is small in this case, the two-photon event topology is similar to the signal event topology. The PYTHIA 5.7 [8] Monte Carlo generator was used for generating events from two-photon processes where the Q^2 of both photons is smaller than 1.3 GeV^2 and the invariant mass of the photon-photon system ($M_{\gamma\gamma}$) is greater than 3 GeV. For events with higher Q^2 the generator TWOGEN [12] was used. Event samples for all the possible processes (final state hadrons from point-like $\gamma\gamma \to q\bar{q}$ processes and from vector meson dominance, and all $e^+e^-\ell^+\ell^-$ final states) were generated. Two-photon events were not generated in the region $Q^2 < 1.3$ GeV^2 and $M_{\gamma\gamma} < 3$ GeV. This region did not represent a serious background to the search presented here.
- Events from the four-fermion processes $\ell^+\ell^- q\bar{q}$, $\ell\nu_\ell q\bar{q}'$, $\nu_\ell\bar{\nu}_\ell q\bar{q}$ and $\nu\bar{\nu}\ell^+\ell^-$ are a serious background for the $L^0\bar{L}^0$ and L^+L^- searches. The EXCALIBUR generator was used to generate all four-fermion processes [13].

Generated signal and background events were processed through the full simulation of the OPAL detector [14], and the same event analysis chain was applied to these simulated events as to the data.

3. Data analysis

Charged particle tracks were selected with the same track quality requirements as in Refs. [15,16], except that in order to allow a large acceptance for long lived L^- and L^0 candidates whose flight lengths are up to $\approx$ 10 cm, the $|d_0|$ cut was loosened from 2.5 cm to 8.0 cm, where $|d_0|$ is the distance of closest approach to the interaction point in the plane perpendicular to the beam axis. The rest of the criteria were as follows. Tracks were required to have at least 20 measured spatial hits, more than 50% of the hits geometrically expected, and a transverse momentum exceeding 100 MeV. Electromagnetic clusters in the barrel region were required to have an energy of at least 170 MeV, and the clusters in the endcaps to have an energy of at least 250 MeV and to contain at least two adjacent lead glass blocks. Clusters in the hadron calorimeters were required to have an energy of at least 0.6 GeV in the barrel and endcaps, and at least 2 GeV in the pole tips detectors. Background from cosmic rays was suppressed by requiring at least one track to have a hit in the TOF counter within 10 ns of the expected time-of-flight.

Event observables such as the total visible energy or hemisphere momenta were calculated as follows. An energy cluster in the calorimeters is defined to be associated with a central detector track if the difference in polar angle is less than 0.1 rad and the difference in azimuthal angle is less than 0.1 rad. The track momenta and the momentum vectors of EM or HCAL calorimeter clusters not associated with charged tracks were first summed. When a calorimeter cluster was associated to charged tracks, the scalar sum of the as-

Table 1
The numbers of events remaining (in the $L^0\bar{L}^0$ search), normalised to the integrated luminosity, are compared with the data after each cut for various background processes. Numbers are also given for three samples of simulated $L^0\bar{L}^0$ events. The numbers of events expected from two-photon processes ('$\gamma\gamma$') do not include the region $M_{\gamma\gamma} < 3$ GeV with $Q^2 < 1.3$ GeV^2.

Case (A)	Data	Total bkg.	$q\bar{q}(\gamma)$	$\ell\ell(\gamma)$	'$\gamma\gamma$'	4-f	$L^0\bar{L}^0$		
m_{L^0} (GeV) decay mode							50 tau	60 muon	60 electron
no cuts	–	–	1645	6458	105k	20.2	15.9	7.61	7.61
cut (A1)	43.0k	29.8k	1604	65.9	28.1k	13.6	15.7	7.49	7.44
cut (A2)	9581	10.7k	1219	59.7	9397	10.9	13.3	6.89	6.54
cut (A3)	1264	1297	1218	55.4	13.8	10.1	12.9	6.86	6.52
cut (A4)	124	130	127	0.21	0.78	2.48	10.2	5.94	5.62
cut (A5)	0	1.13	0.71	0.08	0.00	0.34	5.03	4.59	4.26
cut (A6)	0	0.70	0.33	0.08	0.00	0.29	4.70	4.43	4.09

sociated charged track momenta was subtracted from the cluster energy before including the cluster to reduce double counting. If the energy of a cluster was smaller than the scalar sum of the associated track momenta, the cluster energy was not used. Information from the hadron calorimeter was included in all energy and momentum calculations described below unless otherwise indicated.

3.1. Selection of $L^0\bar{L}^0$ candidates

The following event selection criteria were applied. The numbers of remaining events after each cut are listed in Table 1, for data and for simulated background and signal samples.

(A1) The number of tracks was required to be at least four, and the ratio of the number of tracks which satisfied the selection criteria to the total number of reconstructed tracks was required to be larger than 0.2 in order to reject beam-gas and beam-wall backgrounds.

(A2) In order to reduce the background from two-photon processes and multihadronic events in which one of the jet axes was close to the beam direction, the total energy deposited in each silicon tungsten calorimeter was required to be less than 5 GeV. Furthermore the energy was required to be less than 2 GeV in each forward calorimeter and less than 5 GeV in each side of the gamma-catcher. In addition, the cosine of the polar angle of the thrust axis ($|\cos\theta_{\text{thrust}}|$) was required to be less than 0.95 in order to reduce beam-gas and beam-wall background events as well as events from two-photon processes.

(A3) The visible energy was required to be greater than $0.4\sqrt{s}$ to reduce background from two-photon processes.

(A4) The number of jets was required to be greater than or equal to four. Jets were formed using the Durham algorithm [17] with a jet resolution parameter of $y_{\text{cut}} = 0.006$. With this requirement a large fraction of the multihadron background was removed. The distributions of the number of jets after cut (A3) are shown in Fig. 1a for the data and the simulated background events, and in Fig. 1b for the simulated $L^0\bar{L}^0$ events.

(A5) The number of isolated leptons (e, μ or τ) was required to be at least two. The selection criteria for isolated leptons are listed below.

The momentum of an electron or muon candidate was required to be less than 40 GeV and larger than 2 GeV. Electrons were selected using the artificial neural network described in [18]. Muons were identified as the central detector track which gave the best match to a muon chamber track segment [19]. In the region not covered by the muon chambers, muons were identified using the hadron calorimeters as described in [20]. No additional tracks were allowed within a cone of half-angle 15° around an electron or muon track.

The reconstructed jets described above were used to identify taus. A jet was identified as a one-prong tau decay if the following four conditions were satisfied: (1) the jet contained a track with momentum larger than 3 GeV and less than 40 GeV, (2) the momenta of all the other tracks in the same jet were less than

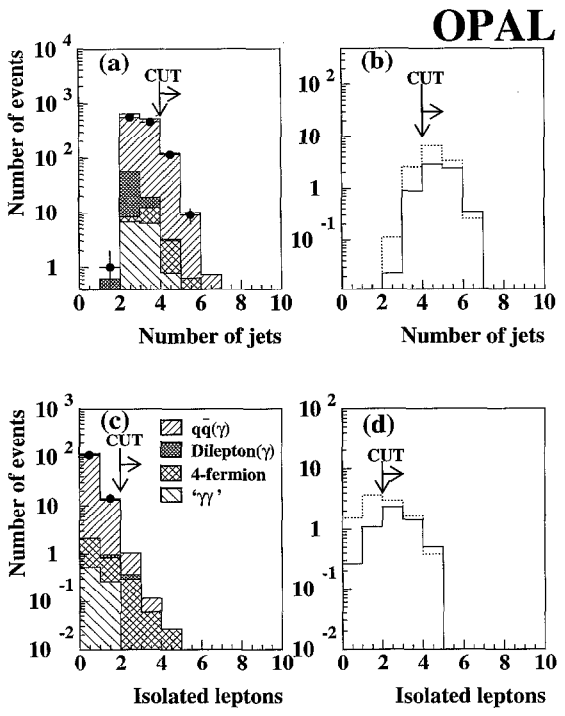

Fig. 1. The distributions of the number of jets after cut (A3) for the data (bold circles with error bars) and for the simulated background events are plotted in (a). The same distributions are shown in (b) for simulated $L^0\bar{L}^0 \to eW^*eW^*$ events with $m_{L^0} = 60$ GeV (solid line histogram) and $L^0\bar{L}^0 \to \tau W^*\tau W^*$ events with $m_{L^0} = 50$ GeV (dotted line histogram). The distributions of the number of isolated leptons after cut (A4) for the data and the simulated background events are displayed in (c). The distributions of the number of isolated leptons for the $L^0\bar{L}^0$ events are shown in (d) for the same samples as (b). The symbols used for the various backgrounds in (a) and (c) are explained in (c).

1 GeV, (3) no other track was found within a cone of half-angle 15° around the high momentum track, and (4) the invariant mass calculated from the track and all cluster momenta within the cone was less than 2.5 GeV. A jet was identified as a three-prong tau decay if the following three criteria were satisfied: (1) there were only three tracks in the jet and all three tracks were inside a cone of half-angle 15° around the jet axis, (2) the vector sum of the three charged particle momenta had magnitude greater than 3 GeV, and (3) the invariant mass of all tracks and clusters within the cone was less than 2.5 GeV.

The distributions of the number of isolated leptons after cut (A4) are plotted in Fig. 1c for the data and the simulated background events, and in Fig. 1d for the simulated $L^0\bar{L}^0$ events.

(A6) The invariant mass of the two isolated leptons with the largest momenta was required to be larger than 10 GeV. This cut rejected multihadron events with two lepton candidates in a single jet.

No events were observed in the data after the above selection. This result was consistent with the number of expected background events of 0.70. The detection efficiency for $L^0\bar{L}^0$ events was calculated for six m_{L^0} values between 40 and 63 GeV. The efficiency for m_{L^0} in the range of 50–63 GeV was about 50–60% for $L^0\bar{L}^0 \to eW^*eW^*$ or $\mu W^*\mu W^*$ events, and about 30% for $L^0\bar{L}^0 \to \tau W^*\tau W^*$ events.

These analysis criteria have a sensitivity for tagging all light leptons (e, μ and τ). The three different final states of $L^0\bar{L}^0 \to eW^* + eW^*$, $\mu W^* + \mu W^*$ and $\tau W^* + \tau W^*$ were considered in calculating efficiencies. If the decay products of $L^0\bar{L}^0$ were mixed ($L^0\bar{L}^0 \to eW^*\mu W^*$, $eW^*\tau W^*$ or $\mu W^*\tau W^*$), the efficiencies would have values intermediate between the cases considered here. The efficiencies for the $L^0\bar{L}^0 \to \tau W^*\tau W^*$ case were the lowest in this analysis, and hence lead to the most conservative limit. The trigger efficiency was 100% for the selected signal events.

3.2. *Selection of* L^+L^- *candidates*

Similar cuts were applied to select the signal events for case (B): $L^- \to \nu_L W^{*-}$ and case (C): $L^- \to \nu_\ell W^{*-}$; however, some cut values were optimised differently for the two cases. The number of events remaining after each cut are listed in Table 2 for case (B) and in Table 3 for case (C). For comparison both tables also include the corresponding numbers of simulated background and L^+L^- events.

The following selection criteria were applied:

(B1), (C1) The number of charged tracks was required to be at least two, and the ratio of the number of tracks which satisfied the selection criteria to the total number of reconstructed tracks was required to be greater than 0.2.

(B2), (C2) The criteria for energy deposits in the silicon tungsten calorimeter, the forward calorimeter and the gamma-catcher were identical to those in the $L^0\bar{L}^0$ analysis. The cosine of the polar angle of the thrust axis ($|\cos\theta_{\text{thrust}}|$) was required to be less than 0.9. The $|\cos\theta_{\text{thrust}}|$ cut is harder than in the L^0 analysis because the acoplanarity angle, which is discussed

Table 2
The numbers of events remaining, normalised to the integrated luminosity of the data, for various background processes are compared with data after each cut for the $L^- \to \nu_L W^{*-}$ case. Numbers of expected events are also given for three samples of simulated L^+L^- events. The numbers of events expected from two-photon processes do not include the region $M_{\gamma\gamma} < 3$ GeV with $Q^2 < 1.3$ GeV^2.

case (B)	Data	Total bkg.	$q\bar{q}(\gamma)$	$\ell\ell(\gamma)$	'$\gamma\gamma$'	4-f	L^+L^-		
m_{L^-} (GeV)							63	60	55
m_{ν_L} (GeV)							55	45	45
no cuts	–	–	1645	6458	105k	20.2	10.6	15.8	22.4
cut (B1)	123k	47.1k	1606	963	44.5k	18.0	10.2	15.3	21.8
cut (B2)	50.5k	16.4k	1142	839	14.4k	11.1	9.42	14.0	19.7
cut (B3)	748	780	593	168	12.2	6.58	4.95	11.9	13.9
cut (B4)	379	421	299	112	5.46	4.89	4.77	10.9	12.9
cut (B5)	289	340	231	98.5	5.46	4.76	4.77	10.9	12.9
cut (B6)	13	14.9	0.06	9.14	4.68	1.06	4.77	10.9	12.8
cut (B7)	8	7.44	0.06	2.16	4.16	1.06	4.77	10.8	12.7
cut (B8)	0	1.36	0.06	0.12	1.04	0.14	4.09	9.47	10.7
dijet	0	1.27	0.06	0.11	1.04	0.06	3.03	7.84	9.31
cut (B10)	0	0.35	0.00	0.03	0.26	0.06	2.82	6.92	8.39
monojet	0	0.09	0.00	0.01	0.00	0.08	1.06	1.63	1.43
(B10)+monojet	0	0.44	0.00	0.04	0.26	0.14	3.88	8.55	9.82

Table 3
The numbers of events remaining, normalised to the integrated luminosity, for various background processes are compared with data after each cut for the $L^- \to \nu_\ell W^{*-}$ case. Numbers of expected events are also given for three samples of simulated L^+L^- events. The numbers of events expected from two-photon processes do not include the region $M_{\gamma\gamma} < 3$ GeV with $Q^2 < 1.3$ GeV^2.

Case (C)	Data	Total bkg.	$q\bar{q}(\gamma)$	$\ell\ell(\gamma)$	'$\gamma\gamma$'	4-f	L^+L^-		
m_{L^-} (GeV)							45	55	63
no cuts	–	–	1645	6458	105k	20.2	32.7	22.4	10.6
cut (C1)	123k	47.1k	1606	963	44.5k	18.0	32.0	22.1	10.5
cut (C2)	50.5k	16.4k	1142	839	14.4k	11.1	27.6	19.1	9.29
cut (C3)	237	245	195	46.5	1.04	2.95	21.5	15.5	7.44
cut (C4)	161	169	129	37.3	0.52	2.46	19.0	14.0	6.81
cut (C5)	136	138	110	25.4	0.52	2.43	16.0	11.6	6.80
cut (C6)	38	49.2	26.6	22.0	0.00	0.58	15.7	11.5	5.57
cut (C7)	20	31.1	26.6	3.95	0.00	0.58	15.5	11.5	5.53
cut (C8)	7	6.99	6.26	0.39	0.00	0.34	12.8	9.71	4.76
dijet	7	6.98	6.26	0.38	0.00	0.34	11.7	8.99	4.26
cut (C9)	4	4.84	4.50	0.17	0.00	0.17	10.7	7.90	3.87
cut (C10)	0	0.50	0.33	0.08	0.00	0.09	9.62	7.31	3.33
monojet	0	0.01	0.00	0.01	0.00	0.00	1.14	0.72	0.50
(C10)+monojet	0	0.51	0.33	0.09	0.00	0.09	10.8	8.03	3.83

later, becomes unreliable if the jet axes are too close to the beam direction.

(B3), (C3) Events from two-photon processes with a small visible energy were efficiently reduced by demanding the event transverse momentum (P_t) calculated excluding the hadron calorimeter clusters to be larger than 4 GeV and the transverse momentum (P_t^{HCAL}) calculated including the hadron calorimeter clusters to be larger than 5 GeV in case (B) (cut B3). Although most of the events from two-photon processes were rejected by the P_t cut, the P_t^{HCAL} cut was applied to reject occasional events with a high

transverse momentum neutral hadron. In case (C), the transverse momentum was expected to be larger, hence P_t and P_t^{HCAL} were required to be larger than 10 GeV and 12 GeV, respectively (cut C3).

(B4), (C4) "Radiative return" events from $e^+e^- \to Z\gamma$, where the γ escaped close to the beam direction, were rejected by requiring that the polar angle of the missing momentum direction θ_{miss} satisfy $|\cos\theta_{\mathrm{miss}}| < 0.8$.

(B5), (C5) If an electromagnetic cluster was not accompanied by any track within a cone of half-angle 25° around its direction, it was defined to be an isolated photon. Events with an isolated photon of energy greater than 15 GeV were rejected for case (B) (cut B5). For case (C) the energy cut was increased to 25 GeV (cut C5). The cut values were optimized to maintain high efficiency for the signal. This cut rejects some $e^+e^- \to Z\gamma$ events.

(B6), (C6) A visible energy cut was applied to reduce both multihadron and four-fermion background. The visible energy of L^+L^- events in case (B) was expected to be smaller than about 50 GeV, since the two heavy ν_L's carry away a significant fraction of the energy. The visible energy was required to be smaller than $0.35\sqrt{s}$ for case (B) (cut B6). In case (C), on the other hand, the visible energy was required to be larger than $0.3\sqrt{s}$ and smaller than $0.8\sqrt{s}$ (cut C6). The visible energy distributions before this cut are shown in Fig. 2.

(B7), (C7) Events which were kinematically consistent with $\tau^+\tau^-(\gamma)$ were rejected. The tracks and the clusters in an event were divided into two hemispheres defined by the plane perpendicular to the thrust axis. Events were identified as $\tau^+\tau^-(\gamma)$ if the charged multiplicities in the two thrust hemispheres were a single track in one hemisphere and either one or three tracks in the opposite hemisphere, the sum of the charged particle momenta in one of the hemispheres was greater than 10 GeV, and the charged particle masses of both hemispheres were smaller than the τ mass. Assuming that the event was a $\tau^+\tau^-(\gamma)$, the maximum value of the acoplanarity angle was calculated from the absolute value of the charged particle momentum sum in each hemisphere. If the measured acoplanarity angle was smaller than this calculated maximum value, the event was considered to be a $\tau^+\tau^-(\gamma)$ and rejected. The acoplanarity angle ϕ_{acop} was defined as $\pi - \phi_{\mathrm{open}}$, where ϕ_{open} is the azimuthal opening angle between the directions of the momentum sums of the particles in the two thrust hemispheres.

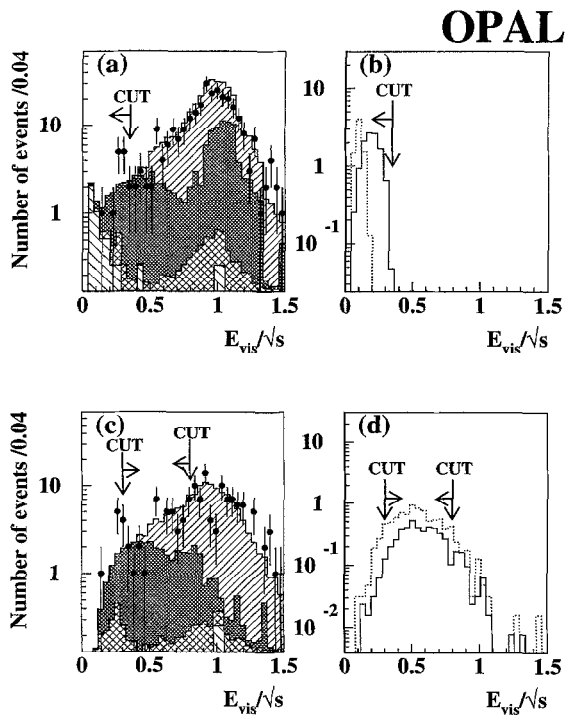

Fig. 2. The distributions of visible energy plotted for data (bold circles with error bars) and various simulated background processes after cut (B5) for case (B) or (C5) for case (C) are shown in (a) and (c), respectively. The symbols used for the various backgrounds are the same as in Fig. 1. In (b) the solid and dotted histograms represent simulated L^+L^- events with $L^- \to \nu_L W^{*-}$ decay for (m_{L^-}, m_{ν_L}) = (60 GeV, 45 GeV) and (63 GeV, 55 GeV), respectively. In (d) the solid and dotted histograms represent simulated L^+L^- events with $L^- \to \nu_\ell W^{*-}$ decay for m_{L^-} = 60 GeV and 45 GeV, respectively.

(B8), (C8) In order to reject events containing two back-to-back jets or leptons, the thrust of the events was required to be less than 0.9.

Events were classified into two different categories according to the following criteria. If one of the hemispheres had an energy smaller than 1 GeV and contained no good track, the event was categorised as a monojet event; otherwise the event was classified as a dijet event. All the events classified as monojet events were considered to be heavy lepton candidates.

(C9) For dijet events in case (C), the remaining background comes primarily from hadronic events in which a mismeasurement of the energy of a jet leads to an ar-

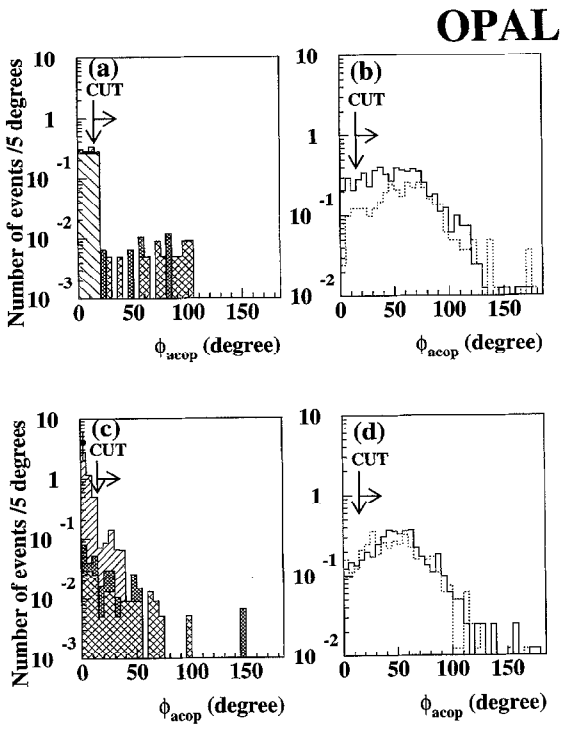

Fig. 3. The acoplanarity angle distributions are shown for data and simulated background events after cut (B8) for case (B) or (C9) for case (C) are plotted in (a) and (c), respectively. No events survived at this stage for the data in case (B). The symbols used for various backgrounds are the same as for Fig. 1. In (b) the solid and dotted histograms represent simulated L^+L^- events with $L^- \to \nu_L W^{*-}$ decays for (m_{L^-}, m_{ν_L}) = (60 GeV, 45 GeV) and (63 GeV, 55 GeV), respectively. In (d) the solid and dotted histograms represent simulated L^+L^- events with $L^- \to \nu_\ell W^{*-}$ decays, for m_{L^-} = 60 GeV and 45 GeV, respectively.

tificial missing momentum. This missing momentum tends to lie along the direction of jets in ordinary multihadron events. The total energy sum (E_{back}) within a cone of 30° half-angle around the direction of the missing momentum was calculated. In case (C) we required E_{back} to be less than 3 GeV. In case (B) the E_{back} cut was not used because multihadron events were sufficiently reduced by cut (B6).

(B10), (C10) The acoplanarity angle (ϕ_{acop}) between the two jets was required to be greater than 15°. The acoplanarity angle distributions just before the cut are shown in Fig. 3.

No event was observed in the data after the above selections. These results were consistent with the expected background from all sources of 0.44 events for case (B) and 0.51 events for case (C).

The detection efficiencies for L^+L^- events were calculated at $\sqrt{s}$ = 130 and 136 GeV. In case (B), the efficiency was about 55% for (m_{L^-}, m_{ν_L}) = (60 GeV, 45 GeV), and 40% for (63 GeV, 55 GeV). In case (C) the efficiency was at least 33% for m_{L^-} in the range 45–63 GeV. The trigger efficiency was 100% for the selected signal events.

4. Mass limits

The expected numbers of neutral and charged heavy lepton events were estimated for various values for heavy lepton mass (or combinations of (m_{L^-}, m_{ν_L})) using the detection efficiency at each centre-of-mass energy, the cross-section and integrated luminosity. In the calculation of limits the detection efficiency at arbitrary values of the heavy lepton masses was interpolated using a polynomial fit.

The systematic errors on the total number of expected signal events were estimated to be 3–6% from Monte Carlo statistics, depending on the event topology, 1.2% from the interpolation of the efficiencies, 0.9% from the uncertainty in the integrated luminosity, 4.3% from the lepton identification uncertainty for the $L^0\bar{L}^0$ case, and 1.5% (0.6%) from the uncertainty in the fragmentation of W* hadronic decays for $L^0\bar{L}^0$ (L^+L^-). The fragmentation errors arose through the jet reconstruction and lepton isolation uncertainties for the $L^0\bar{L}^0$ case and mainly through the uncertainty in the estimation of the acoplanarity angle and the missing momentum direction for the L^+L^- case. The fragmentation error was estimated by varying the optimized fragmentation parameters [21] in the JETSET 7.4 Monte Carlo generator. The systematic error due to trigger efficiency was estimated to be negligible for the selected signal events. In calculating the mass limits the systematic errors were treated as in Ref. [22] and were considered to be independent.

A 95% C.L. lower limit of 62.5 GeV is obtained for the Dirac neutral heavy lepton mass, assuming that both L^0 and $\bar{L}^0$ decay into eW* with 100% branching fraction. The mass limits for the cases of $L^0 \to \mu W^*$ and $L^0 \to \tau W^*$ are 63.0 GeV and 57.4 GeV, respectively. For Majorana L^0 the limits are reduced to 51.4 GeV for the eW* decay, 52.2 GeV for μW^* decay and 44.2 GeV for τW^* decay due to the smaller cross-section near the $L^0\bar{L}^0$ threshold.

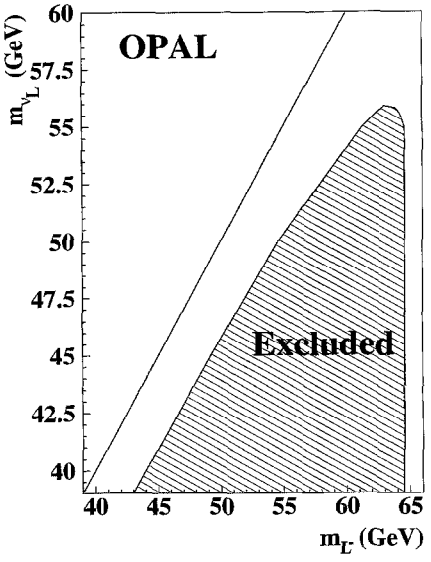

Fig. 4. The excluded region in this analysis in the (m_{L^-}, m_{ν_L}) plane for case (B). If L^- decays into $\nu_L + W^{*-}$ and ν_L is assumed to be a stable heavy neutrino, the hatched region is excluded with more than 95% C.L. The region $m_{\nu_L} < 45$ GeV is already excluded for the Dirac ν_L and $m_{\nu_L} < 39.5$ GeV for the Majorana ν_L from the upper limit of the Z^0 decay width measurements at LEP [3]. The diagonal line shows $m_{L^-} = m_{\nu_L}$.

The mass of $L^{\pm}$ was found to be larger than 64.5 GeV at 95% C.L. for case (B), if $m_{L^-} - m_{\nu_L} > 10$ GeV. The excluded region in the (m_{L^-}, m_{ν_L}) plane for case (B) is presented in Fig. 4. For case (C) the lower limit for m_{L^-} is 63.9 GeV at 95% C.L.

5. Summary and conclusions

A search has been made for pair production of unstable neutral and charged heavy leptons using a data sample corresponding to an integrated luminosity of 2.6 pb^{-1} at $\sqrt{s}$ = 130 GeV and 2.6 pb^{-1} at $\sqrt{s}$ = 136 GeV, collected with the OPAL detector at LEP. No event remained after the selection cuts, consistent with the expected number of background events.

The 95% C.L. lower limit on the Dirac L^0 mass, assuming that L^0 decays into eW* with 100% branching fraction, was obtained to be 62.5 GeV. The mass limits for μW^* and τW^* decays are 63.0 GeV and 57.4 GeV, respectively. For Majorana L^0 the limits were reduced to 51.4 GeV for pure eW* decay, 52.2 GeV for pure μW^* decay and 44.2 GeV for the τW^* case due to the smaller cross-section in the region near the $L^0\bar{L}^0$ threshold.

The excluded region in the (m_{L^-}, m_{ν_L}) plane is presented in Fig. 4. If $m_{L^-} - m_{\nu_L} > 10$ GeV, the mass of L^- was found to be larger than 64.5 GeV at 95% C.L. If $m_{\nu_L} > m_{L^-}$ and L^- decays into a massless neutrino and a virtual W boson, a lower limit of 63.9 GeV at 95% C.L. was obtained for m_{L^-}. The results of these analyses are consistent with, and in some cases have extended, existing limits from other LEP experiments [3,4].

Acknowledgements

We particularly wish to thank the SL Division for their efficient operation of the LEP accelerator and for their continuing close cooperation with our experimental group. In addition to the support staff at our own institutions we are pleased to acknowledge the
Department of Energy, USA,
National Science Foundation, USA,
Particle Physics and Astronomy Research Council, UK,
Natural Sciences and Engineering Research Council, Canada,
Israel Ministry of Science,
Israel Science Foundation, administered by the Israel Academy of Science and Humanities,
Minerva Gesellschaft,
Japanese Ministry of Education, Science and Culture (the Monbusho) and a grant under the Monbusho International Science Research Program,
German Israeli Bi-national Science Foundation (GIF),
Direction des Sciences de la Matière du Commissariat à l'Energie Atomique, France,
Bundesministerium für Bildung, Wissenschaft, Forschung und Technologie, Germany,
National Research Council of Canada,
Hungarian Foundation for Scientific Research, OTKA T-016660, and OTKA F-015089.

References

[1] L. Montanet et al., Phys. Rev. D 50 (1994) 1418.

[2] H. Baer et al., in Physics at LEP, Vol. 1, eds. J. Ellis and R. Peccei, CERN Yellow Book CERN-86-02 (1986) 297.
[3] ALEPH Collab., D. Decamp et al., Phys. Lett. B 236 (1990) 511;
OPAL Collab., M.Z. Akrawy et al., Phys. Lett. B 240 (1990) 250; B 247 (1990) 448;
L3 Collab., B. Adeva et al., Phys. Lett. B 251 (1990) 321;
OPAL Collab., G. Alexander et al., Z. Phys. C 52 (1991) 175;
DELPHI Collab., P. Abreu et al., Phys. Lett. B 274 (1992) 230.
[4] L3 Collab., M. Acciarri et al., CERN-PPE/96-038 (1996); ALEPH Collab., D. Buskulic et al., CERN-PPE/96-080 (1996).
[5] OPAL Collab., K. Ahmet et al., Nucl. Instr. Meth. A 305 (1991) 275;
P.P. Allport et al., Nucl. Instr. Meth. A 324 (1993) 34; A 346 (1994) 476.
[6] B.E. Anderson et al., IEEE Transactions on Nuclear Science 41 (1994) 845.
[7] S. Jadach and J. Kühn, preprint MPI-PAE/PTh 64/86.
[8] T. Sjöstrand, Comput. Phys. Commun. 82 (1994) 74.
[9] F.A. Berends, K. Kleiss and S. Jadach, Nucl. Phys. B 202 (1982) 63; Comp. Phys. Comm. 29 (1983) 185.
[10] S. Jadach, B.F.L. Ward, Z. Wąs, Comp. Phys. Comm. 79 (1994) 503.
[11] M. Böhm, A. Denner and W. Hollik, Nucl. Phys. B 304 (1988) 687;
F.A Berends, K. Kleiss and W. Hollik, Nucl. Phys. B 304 (1988) 712.
[12] A. Buijs et al., Comp. Phys. Comm. 79 (1994) 523.
[13] F.A Berends, K. Kleiss and R. Pittau, Comp. Phys. Comm. 85 (1995) 437.
[14] J. Allison et al., Nucl. Instr. Meth. A317 (1992) 47.
[15] OPAL Collab., G. Alexander et al., CERN-PPE/96-019 (1996), to be published in Physics Letters.
[16] OPAL Collab., G. Alexander et al., CERN-PPE/96-020 (1996), to be published in Physics Letters.
[17] S. Catani et al., Nucl. Phys. B269 (1991) 432.
[18] OPAL Collab., R. Akers et al., Phys. Lett. B 327 (1994) 411.
[19] OPAL Collab., P. Acton et al., Z. Phys. C 58 (1993) 523.
[20] OPAL Collab., R. Akers et al., Z. Phys. C 60 (1993) 199.
[21] OPAL Collab., G. Alexander et al., Z. Phys. C 69 (1996) 543.
[22] R.D. Cousins and V.L. Highland, Nucl. Inst. and Methods A 320 (1992) 331.